The myosin interacting-heads motif present in live tarantula muscle explains tetanic and posttetanic phosphorylation mechanisms

Raúl Padrón[a,1,2], Weikang Ma[b,1], Sebastian Duno-Miranda[c,3], Natalia Koubassova[d], Kyoung Hwan Lee[a,4], Antonio Pinto[c], Lorenzo Alamo[c], Pura Bolaños[e], Andrey Tsaturyan[d], Thomas Irving[b], and Roger Craig[a]

[a]Division of Cell Biology and Imaging, Department of Radiology, University of Massachusetts Medical School, Worcester, MA 01655; [b]Biophysics Collaborative Access Team, Department of Biological Sciences, Illinois Institute of Technology, Chicago, IL 60616; [c]Centro de Biología Estructural, Instituto Venezolano de Investigaciones Científicas, Caracas 1020A, Venezuela; [d]Institute of Mechanics, Moscow State University, 119992 Moscow, Russia; and [e]Centro de Biofísica y Bioquímica, Instituto Venezolano de Investigaciones Científicas, Caracas 1020A, Venezuela

This contribution is part of the special series of Inaugural Articles by members of the National Academy of Sciences elected in 2018.

Contributed by Raúl Padrón, April 7, 2020 (sent for review December 6, 2019; reviewed by H. Lee Sweeney and Rene Vandenboom)

Striated muscle contraction involves sliding of actin thin filaments along myosin thick filaments, controlled by calcium through thin filament activation. In relaxed muscle, the two heads of myosin interact with each other on the filament surface to form the interacting-heads motif (IHM). A key question is how both heads are released from the surface to approach actin and produce force. We used time-resolved synchrotron X-ray diffraction to study tarantula muscle before and after tetani. The patterns showed that the IHM is present in live relaxed muscle. Tetanic contraction produced only a very small backbone elongation, implying that mechanosensing—proposed in vertebrate muscle—is not of primary importance in tarantula. Rather, thick filament activation results from increases in myosin phosphorylation that release a fraction of heads to produce force, with the remainder staying in the ordered IHM configuration. After the tetanus, the released heads slowly recover toward the resting, helically ordered state. During this time the released heads remain close to actin and can quickly rebind, enhancing the force produced by posttetanic twitches, structurally explaining posttetanic potentiation. Taken together, these results suggest that, in addition to stretch activation in insects, two other mechanisms for thick filament activation have evolved to disrupt the interactions that establish the relaxed helices of IHMs: one in invertebrates, by either regulatory light-chain phosphorylation (as in arthropods) or Ca^{2+}-binding (in mollusks, lacking phosphorylation), and another in vertebrates, by mechanosensing.

skeletal muscle | thick filament activation | phosphorylation | posttetanic potentiation | myosin interacting-heads motif

Muscle contraction results from the force exerted by the myosin heads on Ca^{2+}-activated thin filaments, following release of the heads from the thick-filament backbone. We want to understand how the helically ordered heads on the relaxed thick filament sense the Ca^{2+}-activation of the thin filaments so that their release is coordinated with thin filament activation. Initial evidence for such a "thick-filament activation" mechanism was experimentally found in 2015 when mechanosensing was proposed for vertebrate muscle (1). Our first goal here is to inquire if a vertebrate-like mechanosensing mechanism is also present in muscles from invertebrates.

The structure of thick filaments from vertebrate and invertebrate muscle has been studied extensively by electron microscopy (EM) negative staining (2, 3) and low-angle X-ray diffraction (XRD) (4–6). Invertebrate filaments (*Limulus*, scallop, tarantula) were found to be particularly amenable to structural studies, as their heads were well ordered in true helices, in contrast to the poorer ordering in pseudohelices found in vertebrates (7). Three-dimensional (3D) reconstructions from frozen-hydrated tarantula thick filaments showed that the helices of heads on the filaments were formed by a two-headed assemblage that we called the myosin interacting-heads motif (IHM) (8, 9), formed by the interaction of a blocked head (BH) and a free head (FH) (10) with the subfragment-2 (8) (Fig. 1*A*). The head–head interaction was essentially identical to that found in single molecules of myosin II in the relaxed state (10, 11). The switch-2 "closed" state of the myosin head was found to be required for establishing the helical arrangement of IHMs around the thick filament backbone, as shown by XRD (12) and EM (13). The IHM has been found to be present in all animals studied so far by EM of isolated myosin molecules (14, 15) and isolated thick filaments of skeletal, cardiac, and invertebrate smooth muscle (16). In all thick filaments the IHMs are located approximately parallel to the filament axis, the only exception

Significance

Muscle contracts when myosin heads on the thick filaments bind to actin in the thin filaments, producing force, thin filament sliding, and sarcomere shortening. Two important questions on how muscle works are: 1) How myosin heads of a thick filament are "turned on" to enable their binding to actin; and 2) how, after a tetanus, a muscle produces a stronger twitch force than the twitch force produced before the tetanus (posttetanic potentiation). Muscles from tarantula provide insights into both questions: 1) Tarantula thick filaments are not primarily activated by mechanical stress, as in vertebrates, but by phosphorylation; 2) posttetanic potentiation in tarantula muscles occurs by phosphorylated heads that remain released and disordered.

Author contributions: R.P., T.I., and R.C. designed research; R.P., W.M., S.D.-M., N.K., K.H.L., A.P., L.A., P.B., A.T., T.I., and R.C. performed research; R.P., W.M., S.D.-M., N.K., A.P., L.A., P.B., A.T., T.I., and R.C. analyzed data; and R.P., W.M., T.I., and R.C. wrote the paper.

Reviewers: H.S., University of Florida; and R.V., Brock University.

The authors declare no competing interest.

Data deposition: Data for this paper are available in the Open Science Framework repository at https://osf.io/anxuy/?view_only=5491c6ba8bca4add9d97930614734e0e.

[1]R.P. and W.M. contributed equally to this work.

[2]To whom correspondence may be addressed. Email: raul.padron@umassmed.edu.

[3]Department of Molecular Physiology and Biophysics, Cardiovascular Research Institute, University of Vermont, Burlington, VT 05405.

[4]Massachusetts Facility for High-Resolution Electron Cryo-Microscopy, University of Massachusetts Medical School, Worcester, MA 01655.

This article contains supporting information online at https://www.pnas.org/lookup/suppl/doi:10.1073/pnas.1921312117/-/DCSupplemental.

First published May 22, 2020.

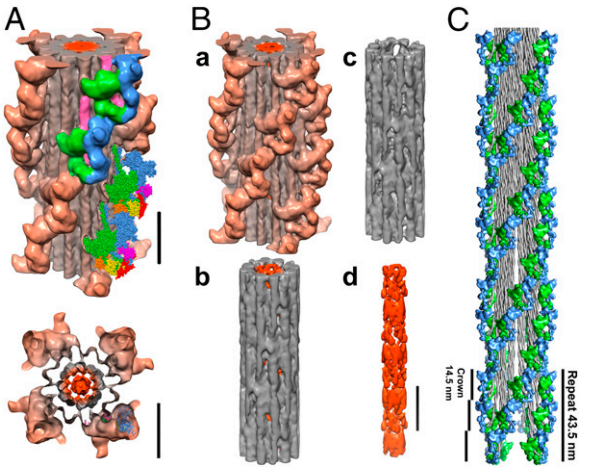

Fig. 1. Tarantula thick-filament 3D reconstruction and model for interpreting XRD patterns. (*A*) Longitudinal and transverse views of 2.0-nm resolution frozen-hydrated 3D map [EMD-1950 (20)] showing densities of four helices of myosin heads forming IHMs (tan). Two IHM densities are highlighted with BH (green) and FH (blue), and subfragment-2 (pink). IHMs are arranged every 14.5 nm in crowns, with densities of the backbone including myosin tails (gray) and a central PM core (orange). (Scale bar, 14.5 nm.) (*B*) Densities of the 3D map composed of (*a*) IHM crowns (tan), and (*b*) a backbone, comprising (*c*) an annulus of tails (gray), and (*d*) a central PM core (orange). (Scale bar, 14.5 nm.) (*C*) Pseudothick filament model with heads represented by PDB 3JBH (shown in *A*), and tails modeled using the tarantula MHCII sequence [GenBank KT619079 (20)].

being insect flight muscle (*Lethocerus*), with a perpendicular IHM (17). The IHM has been key to the concept of super-relaxation (18) and understanding the structural pathogenesis of hypertrophic and dilated cardiomyopathy (19). We show that an IHM-based structure (Fig. 1*C*) [PDB ID code 3JBH (20)] explains the XRD pattern from relaxed skinned tarantula muscle (21). Our second goal here is to assess if the IHM is present in living relaxed tarantula muscle as well as skinned muscle by recording XRD patterns from resting leg muscle in the whole animal (in vivo) or from excised legs (ex vivo).

The modulation of skeletal muscle contraction by myosin light-chain phosphorylation has been extensively studied (22, 23). Studies on purified myosin from *Limulus* skeletal muscle (24) [an arthropod, like tarantula, exhibiting a similar thick-filament structure (25)] showed it was regulated by a Ca^{2+}-calmodulin myosin light-chain kinase (MLCK)-dependent phosphorylation of its myosin regulatory light chain (RLC), and being dephosphorylated by a myosin light-chain phosphatase (MLCP). While myosin from vertebrate skeletal and cardiac muscle can also be phosphorylated, however, there was no direct effect on the in vitro actin-activated Mg-ATPase activity (26). In purified myosin from tarantula muscle, unlike *Limulus*, phosphorylation does not directly regulate myosin activity but is associated with enhanced actin-activated myosin Mg-ATPase activity (27). EM of negatively stained thick filaments showed that RLC phosphorylation induced the release and disordering of the helically ordered heads (27), consistent with changes in the equatorial X-ray intensities from skinned tarantula muscle (28) and with similar studies of *Limulus* (29) and rabbit skeletal muscle (30, 31). Thus, in vitro, release of heads upon phosphorylation is associated with either switching on of thick filament activity (*Limulus*) or enhancement of thick filament activity (tarantula and vertebrate). Further structural studies showed that tarantula thin filaments are regulated by actin/tropomyosin, as in vertebrate skeletal muscle (32).

Tarantula muscle has a phosphorylatable RLC (27) that can be mono- or biphosphorylated (33) on serines Ser35 and Ser45, as detected by mass spectrometry (MS) (34). On this basis, an IHM-based phosphorylation mechanism was proposed in which phosphorylation of the FH makes possible phosphorylation of the BH from the next myosin molecule along the helix, the so called cooperative phosphorylation activation (CPA) mechanism (34, 35), which can account for the thick-filament structural changes we observed in tarantula filament homogenates upon Ca^{2+}-activation (27). In this mechanism (Fig. 2*B*), the selective action of MLCK on the RLC of the BH and FH (Fig. 2*A*) allow their sequential cooperative release from the thick-filament backbone by Ser35/Ser45 mono- or biphosphorylation (Fig. 2*B*).

The CPA mechanism (Fig. 2*B*) proposes that the FHs of relaxed muscle are constitutively monophosphorylated (mono-P) by PKC on Ser35 (34) (Fig. 2 *B*, *a*), supported by our ^{18}O MS studies that show that on Ca^{2+}-activation, de novo ^{18}O-ATP incorporation occurs only on Ser45 but not on Ser35 (36). In vitro motility assays show that unregulated rabbit F-actin filaments slide along relaxed isolated thick filaments of tarantula muscle in the absence of Ca^{2+} (34). We therefore proposed that the Ser35 mono-P allows the FHs to move away from and toward the filament backbone by Brownian motion, becoming so-called swaying heads (Fig. 2 *B*, *a*, double curved arrows) (34). Constitutively ON heads (1) [or sentinel heads (37)], functionally similar to the swaying heads of tarantula, have also been hypothesized for vertebrate thick filaments, supported by in vitro motility evidence (38). In the CPA model, the BHs are non-phosphorylated because of steric blocking of their Ser35 by the FHs (Fig. 2 *B*, *a*) (34, 35). In the presence of Ca^{2+} (Fig. 2 *B*, *b*), thin filaments become activated, and the swaying (Ser35 mono-P) FHs produce initial force. Simultaneously, Ca^{2+} activates MLCK and the FHs slowly become phosphorylated on Ser45 (adding to their Ser35 phosphorylation, so that they are fully released from the filament backbone) (Fig. 2 *B*, *c*). These biphosphorylated heads cannot dock back to the filament as their RLC N-terminal extensions (NTEs) containing the phosphorylatable Ser45s are elongated (39) and rigid (40) (Fig. 2 *B*, *c*), which can only be reversed by dephosphorylation by MLCP. This semipermanent release of the FHs removes the steric hindrance of the BH Ser45, so that some BHs become mono-P by MLCK on Ser45 and are released and sway away (due to the mono-P) from the filament backbone (Fig. 2 *B*, *d*) and are now able to produce additional force (Fig. 2 *B*, *e*). Brito et al. (34) suggested that this mechanism may be limited to arthropods, which—as with tarantula—also exhibit RLCs with long NTEs having consensus sequences for two constitutive/potentiating (PKC/MLCK) phosphorylatable serine pairs, in contrast with vertebrate muscles, with short NTEs and a single MLCK-phosphorylatable serine. As the CPA mechanism was devised in the context of filament homogenates or isolated filaments, our third goal here was to test it in live muscle by assessing its structural predictions, using time-resolved synchrotron XRD patterns during a tetanus to evaluate the location and disorder of the heads, and measuring the non-, mono-, and bi-P RLC phosphorylation using urea-glycerol (U-G) gels.

It has been known for over 150 y (41) that force produced by skeletal muscle can be potentiated by its previous activity. There have been several explanations proposed for this so-called posttetanic potentiation (PTP), with the early work reviewed in ref. 42. The potentiation of force in vertebrate skeletal muscle stimulated either at lower frequency (*treppe* or staircase) or higher frequencies resulting in fused tetani (reviewed in refs. 22, 23, and 43), as well as postactivation potentiation and post-activation performance enhancement in human muscle (reviewed in ref. 44), remain an important target of physiological and biophysical research. Our last goal here was to explore the structural basis of PTP in tarantula muscles using XRD.

Here we report: 1) That in thick filaments of live tarantula muscle, the backbone elongation induced by muscle force is

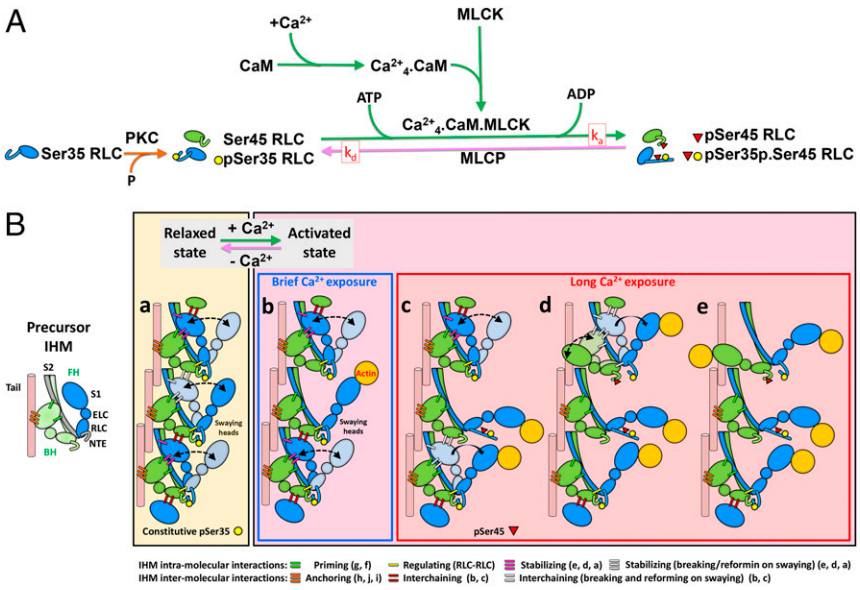

Fig. 2. CPA mechanism proposed for tarantula skeletal muscle. (*A*) Biochemical pathway of myosin RLC phosphorylation/dephosphorylation by MLCK/MLCP. (*B*, *Left*) Precursor IHM with FH (blue) and BH (green), both with non-P RLCs. Initially, PKC constitutively mono-Ps FHs at Ser35 creating the relaxed state (*a*), in which FHs can sway away and back by Brownian motion (swaying heads, double curved arrowhead). BHs are not phosphorylated because of steric hindrance from the FH of the next crown. (*b*) In the active state, when [Ca^{2+}] is high for a brief time, swaying FHs can bind actin and produce force. (*c*) If [Ca^{2+}] remains high for a longer time, swaying FHs are biphosphorylated by MLCK on Ser45. These bi-P FHs cannot dock back onto their partner BHs, exposing the Ser45 of the neighbor BHs to allow MLCK to mono-P them at Ser45, so the BHs become swaying heads as well (double curved arrowhead in *d*). (*e*) After a longer [Ca^{2+}] exposure, most FHs are bi-P and BHs Ser45 mono-P.

much smaller than in frog, implying that mechanosensing is either absent or only of minor importance in tarantula thick filament activation; 2) the IHM structure is present in live, relaxed tarantula muscle and fully explains the observed XRD pattern; 3) there is structural evidence in live tarantula muscle for an IHM-based phosphorylation mechanism of thick filament activation; and 4) this mechanism also provides a structural basis for PTP.

Results and Discussion

The IHM Structure Is Present in Relaxed Live Tarantula Muscle. We recorded XRD patterns from muscles of the femur either in the intact, living animal (in vivo), in whole legs removed from the animal (ex vivo), or with the muscle removed from the femur and skinned (Fig. 3 *A*–*C*). The in vivo preparation (Fig. 3*E*) had the advantage that the femur muscles are intact and, in contrast to the ex vivo preparation (Fig. 3*D*), irrigated by hemolymph carrying O_2 and metabolites. The in vivo and ex vivo patterns are essentially identical, displaying (see labels in Fig. 3*A*): nine 43.35-nm–based myosin layer lines (MLL1 to MLL9); three meridional reflections due to the 14.45-nm–based axial separation of myosin heads (M3, M6, M9); four troponin meridional reflections (Tn1 to Tn4) at 37.21, 19.12, 12.76, and 9.56 nm; two actin ∼35.4-nm–based layer lines at 5.9 and 5.1 nm (ALL6 to ALL7); and four equatorial reflections 10, 11, 20, and 30. The myosin layer line intensities (I_{MLL1}-I_{MLL6}) of the ex vivo and skinned XRD patterns (Fig. 4*A*) after background subtraction (45) show peaks at the same reciprocal radii, indicating that skinning has no effect on the average radial position of the myosin heads above the backbone. The axial spacings of the M3 and M6 meridional reflections (S_{M3} and S_{M6}) are 0.11- and 0.05-nm longer, respectively, than in vertebrate (frog) muscle (1), consistent with other invertebrate muscles (46). The M3 and M6 splitting observed in frog, due to the interference between myosin head arrays on opposite ends of the thick filaments (1), was not detected, possibly because the thick filaments in tarantula muscle are much longer, about 4 to 5 μm (47), so that the interference fringes become too close to be resolved (48, 49). Tarantula skeletal muscle lacks the accessory protein MyBP-C (50) so there was no meridional reflection at 44.2 nm.

Analysis of the XRD patterns in relaxed and contracting tarantula muscle is simplified by the almost total absence of lattice sampling [due to random rotational orientations of the thick filaments (5)], unlike vertebrate skeletal muscle where the filament organization gives rise to significant lattice sampling. We used a thick-filament model (Fig. 1*C*), based on a cryo-EM 3D reconstruction that clearly resolves the FHs and BHs of the IHM (Fig. 1 *A* and *B*, *a*), to assess the separate contribution of BHs and FHs to the XRD pattern. To evaluate the correctness of this IHM-based model as a description of the thick-filament structure in the live muscle lattice, we compared the calculated I_{MLL1}-I_{MLL6} (with all FHs docked) of this IHM-based model with those of the ex vivo and skinned relaxed muscle (Fig. 4*A*). We also did the comparison with the densities of the 2.0-nm 3D map, used to fit the 3JBH IHM-based model (20) (Fig. 1 *B*, *a*) and the higher resolution (1.3 nm) (51) thick-filament frozen-hydrated 3D maps (Fig. 4*A* and *SI Appendix*, Fig. S1). The striking similarity of the layer line profiles shows that the average position of the heads above the backbone and their conformation in ex vivo and skinned muscle is very similar to the ones in both cryo-EM 3D density maps and in the 3JBH-derived IHM-based model. The correctness of the fitting of the model to the observed XRD intensities was assessed using the crystallographic *R*-factor (*Materials and Methods*). The *R*-factor for the IHM-based model and the ex vivo data was low (4.9%), while those for the model and the 2.0- and 1.3-nm 3D-map densities were 4.0% and 8.4%, respectively, indicative of generally good fits. There are two significant differences between the observed and calculated layer line profiles: 1) The strong, narrow M3 meridional reflection in both experimental XRD patterns, and 2) the sampling at the positions of the equatorial 10, 11, and 20 reflections in the ex vivo MLL3 (Fig. 4*A*, arrows), caused by the filament lattice in sarcomeres, while all calculations were performed for a single thick filament in the absence of a lattice. The first difference is because the interference of the X-rays scattered by neighboring thick filaments in the ordered lattice results in a higher meridional peak on MLL3, as explained in Koubassova and Tsaturyan (45). The second difference is because the filament lattice in ex vivo is much better ordered than in skinned muscle.

We conclude that in tarantula live muscle, the 3D-maps obtained by cryo-EM and the IHM-based model derived from these maps fully explain the recorded XRD pattern. Thus, the thick filaments in live tarantula muscle have a structure similar or identical to that observed by cryo-EM, in which myosin heads are in the IHM conformation. This contrasts with the conclusion that IHM-based thick filaments are not consistent with XRD

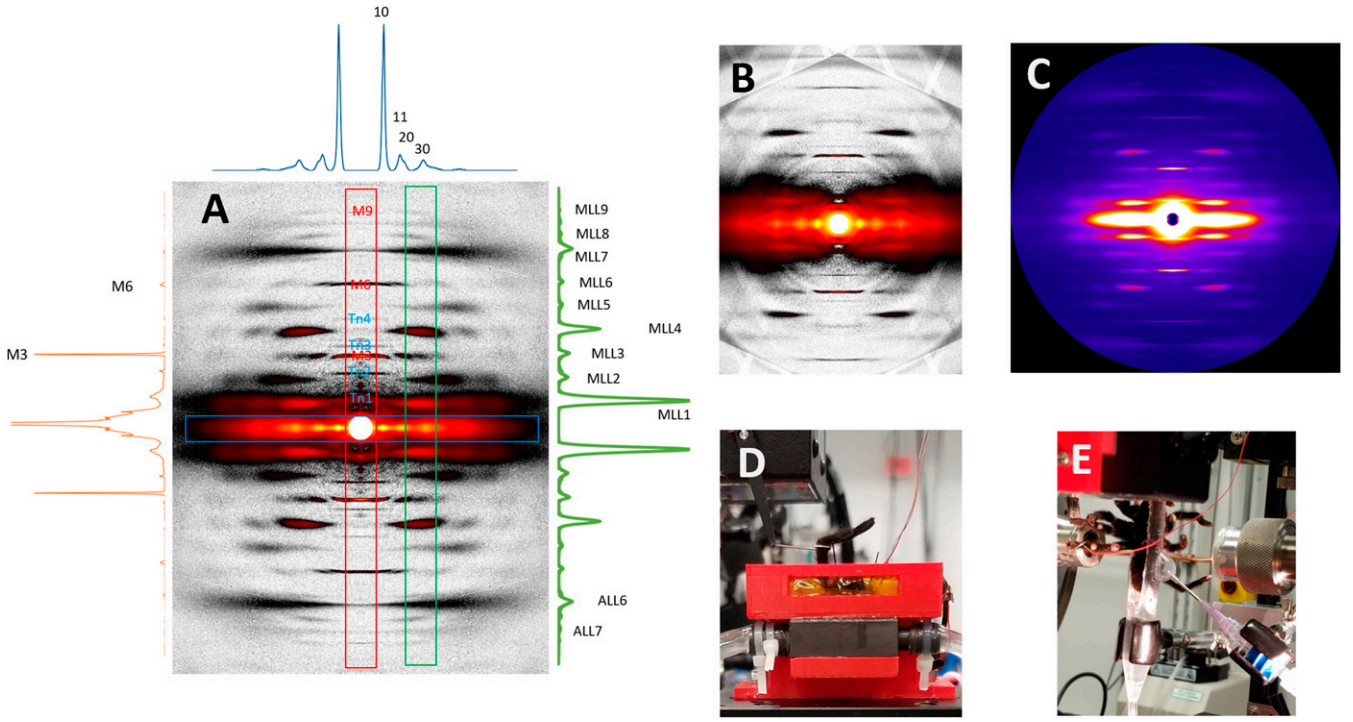

Fig. 3. XRD patterns of muscles of tarantula femurs. (*A*) Ex vivo pattern of resting relaxed femur muscles. Equatorial, meridional and off-meridional intensity profiles in blue (*Top*), orange (*Left*), and green (*Right*); 23 °C, exposure 200 ms. (*B*) Pattern of in vivo femur muscles recorded directly from the femur of an intact live tarantula; 23 °C, exposure 1,000 ms. (*C*) Pattern of a skinned femur muscle in relaxing solution; 23 °C, exposure 1,000 ms. (*D*) Set-up for recording patterns from ex vivo femur (seen through yellow window in chamber), allowing electrical stimulation and tension recording through a metallic linker (hook near the knee) connected to a transducer. (*E*) Set-up for recording patterns from in vivo femur muscle.

patterns of bony fish skeletal muscle and *Lethocerus* flight muscle (52). The reason for this discrepancy is not yet clear, as cryo-EM studies unambiguously show the presence of the IHM structure in isolated, frozen-hydrated *Lethocerus* thick filaments, while no cryo-EM studies have yet been reported on fish thick filaments. Because studies of isolated thick filaments in relaxing conditions from a broad evolutionary range of species show the IHM as a prominent feature (16), our results suggest that it is likely that this will also be the case with all these species in vivo.

Time-Resolved XRD Suggests No Significant Change in Backbone Length in Contracting Tarantula Muscle. In *SI Appendix*, *Supplementary Results*, we show that we can use our 3D tarantula thick-filament reconstructions to demonstrate that the M6 meridional reflection contains information from both the thick-filament backbone and myosin head periodicities (*SI Appendix*, Fig. S1), so changes in S_{M3} can be used as a measure of thick-filament length changes. The time course of S_{M3} (Fig. 5*B*) shows a small, statistically not significant, decrease of 0.02 nm (0.13%) during the tetanus, while S_{M6} (Fig. 5*C*) increases by 0.02 nm (0.27%) during force development (Fig. 5*A*). This increase of S_{M6} in tarantula is much smaller than the 1.8% increase for frog muscle, associated with mechanosensing (49), whereas the 0.13% decrease in S_{M3} in tarantula contrasts with a 1.61% increase in frog. In frog it has been proposed that a small population of constitutively ON motors generates a mechanical stress in the thick filament that lengthens the filament and releases the remaining motors from the OFF state, allowing the development of the full isometric force (1). For tarantula this would imply that the Ser35 mono-P swaying FHs should generate a similar stress releasing the remaining FHs and BHs. However, the lengthening of the tarantula thick-filament backbone as estimated from S_{M6} is only 15% of the lengthening reported for frog. The very small S_{M6} change that we observe in tarantula suggests that the thick-filament backbone in these muscles is very rigid, consistent with the presence of a paramyosin (PM) core that is absent in frog. We conclude that the small change in the S_{M6} and S_{M3} in tarantula compared with frog suggests that a mechanosensing mechanism based on changes in backbone length would, if present, be of minor importance or at a minimum, be very different from the vertebrate mechanism.

The Myosin RLC Is Highly Mono-P and Bi-P during the Tetanic Plateau in Tarantula Muscle. Phosphorylation and dephosphorylation of the myosin regulatory light chains via MLCK, MLCP, and calmodulin has been a common feature of vertebrate and invertebrate skeletal muscle (53), including tarantula (50), since the earliest times of evolution. In tarantula, RLC phosphorylation has been demonstrated using multiple complementary techniques: SDS/PAGE gels (27, 33–35), U-G gels (27, 33–35), autoradiography (27, 33), Western blots using anti-RLC antibodies (35), iso-electric focusing (54), and MS detection of phosphorylatable serines (34–36). RLC phosphorylation was investigated in tarantula filament homogenates using U-G gel electrophoresis, which allows discriminating RLC molecules by their charge as non-P, mono-P, and bi-P, detected as three gel bands (27, 33–35), with the relative quantities of phosphorylated RLC molecules quantified by the relative optical densities of the bands. The BH and FH RLC molecules are distributed between the three bands according to the activation state of the preparation, and their numbers can be accounted for by the CPA mechanism (20). We used a similar approach to determine the phosphorylation levels in rapidly frozen tarantula muscles at the end of a tetanic plateau (*SI Appendix*, Fig. S2 *A*, *b*), showing a substantial increase in mono-P and bi-P and almost complete disappearance of non-P as compared with relaxed live muscles (*SI Appendix*, Fig. S2 *A*, *a* and *B*, *a*). These changes contrast with the ones we have seen on Ca^{2+}-activation in filament

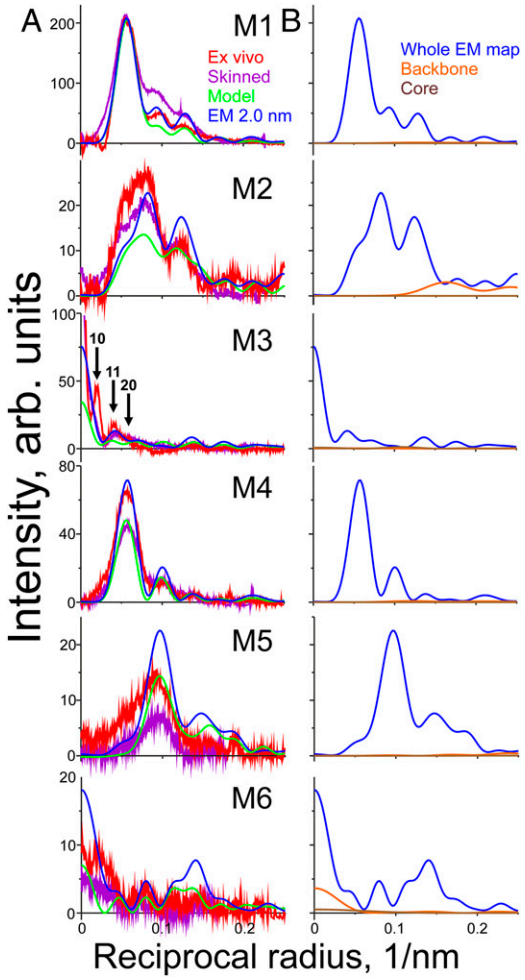

Fig. 4. Comparison of I_{MLL1}-I_{MLL6} profiles with the IHM-based thick-filament model, and frozen-hydrated 3D-map densities. (*A*) I_{MLL1}-I_{MLL6} profiles of ex vivo (red) and skinned (purple) XRD patterns with the IHM-based model (green), and the densities of the 2.0-nm resolution 3D map EMD-1950 (Fig. 1*B*; blue). Note excellent agreement with the strong layer lines (M1 and M4). Imperfect agreement for layer lines 2 and 5 is of minor significance, given the low intensity on these layer lines. Lattice sampling at 10, 11, and 20 is shown by black arrows. (*B*) Comparison of the I_{MLL1}-I_{MLL6} profiles calculated from the 2.0-nm resolution 3D-map densities (blue), with the partial contributions from the backbone alone (orange) and only its PM core (brown).

homogenates (35) (*SI Appendix*, Fig. S2 *B*, *b* vs. *SI Appendix*, Fig. S2 *B*, *a*), suggesting that the MLCK is more effective in the ex vivo muscle because of its higher activity and concentration in the sarcoplasm and possible structural advantages of the sarcomere lattice in vivo (*SI Appendix*, Fig. S3*A*).

Time-Resolved XRD and U-G Gels Add Key Evidence for an IHM-Based Phosphorylation Mechanism. To test the IHM-based CPA mechanism structurally (Fig. 2*B*), we determined the radial distance of the heads from the backbone and their degree of disorder by recording seven time-resolved XRD patterns (Fig. 5) from ex vivo leg muscles. Patterns were recorded before and during a stimulus train that elicited an initial twitch (pretetanic), followed by a tetanus, and then several posttetanic twitches (up to 13.5 s after the end of the tetanus) (Fig. 5 *E*–*H*), and finally 2 to 3, 4 to 5, and >6 min later, during recovery after the stimuli (Fig. 5 *I*–*L*). I_{MLL4}, the second strongest layer line coming from the helical organization of myosin heads was used as a measure of helical order; and a decrease in I_{10} and increase in I_{11+20} were used as indicators of movement of heads away from the thick-filament surface.

During the tetanus plateau, I_{MLL4} decreased to a low (but nonzero) residual value compared to the maximum value before the tetanus (Fig. 5*J*), while I_{10} decreased to a low value (Fig. 5 *F* and *L*) and I_{11} increased to a high value (Fig. 5 *G* and *K*). We conclude that the heads progressively move away from the thick-filament backbone toward the thin filaments during the tetanus and, in the process, become disordered. The presence of residual I_{MLL1} intensity (~20 to 25%) during contraction has been reported in electrically stimulated skeletal muscle from frog (55, 56) and mouse (57) during tetanic contraction and has been interpreted as indicating that during the tetanus plateau ~50% of heads are disordered while ~50% remain ordered in their helical positions as in the resting muscle. Here we interpret the observed residual I_{MLL4} and equatorial changes in tarantula similarly to refs. 55 and 56, but in the context of the CPA mechanism (Fig. 2*B*) and the IHM-based thick-filament structural model (Fig. 1*C*). First, we interpreted the observed XRD pattern changes (Fig. 5) by associating the disordered heads as FHs and the ordered ones as BHs (Fig. 2 *B*, *c*–*e*). We then calculated the effect on I_{MLL1} and I_{MLL4} of progressively removing FHs (*SI Appendix*, Fig. S3*A*; compare with *SI Appendix*, Fig. S3*B*) for interpreting the observed I_{MLL1} and I_{MLL4} changes (Fig. 5). The purpose was to simulate the swaying of the FHs between a docked position in the ordered IHM for a given percentage of the time (t_{IHM}) and a released (disordered) position for the balance of the time (t_{rel}); the duty cycle $[t_{IHM}/(t_{IHM} + t_{rel})]$ for the ensemble of heads would correspond to the fraction of FHs remaining docked in the simulation (*SI Appendix*, Fig. S3*C*), being greatest if the FH spends all of its time in the IHM and least if it spends all of its time released (*SI Appendix*, Fig. S3*C*) (19). The simulation results for I_{MLL1} and I_{MLL4} (*SI Appendix*, Fig. S3*C*) showed residual values of ~34% and 14%, respectively, when all FHs were removed (while all BHs are still present) (*SI Appendix*, Fig. S3*B*), consistent with our proposal that the residual I_{MLL1} and I_{MLL4} come from the (more stable) BH helices (*SI Appendix*, Fig. S3*B*), while all bi-P FHs are disordered during a tetanus. Therefore, we interpret the observed decrease of I_{MLL4} intensity to ~18% (Fig. 5*J*), as reflecting the release and disordering of most FHs while most BHs remain helically ordered. This association is supported also by the observed concomitant changes in I_{10} and I_{11+20} (Fig. 5 *F*–*H*).

We previously found by EM of isolated filaments that RLC phosphorylation induced the release and disordering of the helically ordered heads (27), as shown also by changes in the equatorial reflection intensities from skinned tarantula muscle (28). Similarly, XRD studies on skinned rabbit psoas muscle (31) showed decreases in I_{MLL1} upon RLC phosphorylation, consistent with partial loss of the helical order of myosin heads, and increases in I_{11}/I_{10}, supporting the idea that phosphorylation of myosin RLC causes the myosin heads to move away from the thick filaments toward the thin filaments, thereby enhancing the probability of interaction with actin. Our diffraction (Fig. 5) and U-G gel electrophoresis (*SI Appendix*, Fig. S2 *A*, *b* and *B*, *a*) results in live, intact tarantula muscle are consistent with the proposal that at the end of the plateau (Fig. 2 *B*, *e*), most BHs are Ser45 mono-P (*SI Appendix*, Fig. S2 *A*, *b* and *B*, *a*); that is, the filament-docked non-P BHs become swaying Ser45 mono-P BHs contributing to the X-ray pattern (Fig. 2 *B*, *d*, double curved arrows) with their own docked/released duty cycle (*SI Appendix*, Fig. S3*D*), similar to the swaying Ser35 mono-P FHs in the relaxed state (Fig. 2 *B*, *b*, double curved arrows), while a significant proportion of FHs are bi-P, released and fully disordered.

Previous studies (56, 58, 59) suggested that in frog skeletal muscle, the recovery after a short tetanus takes at least several seconds, and that there was a discrepancy between the fall of tension and the return of myosin heads to their helical paths

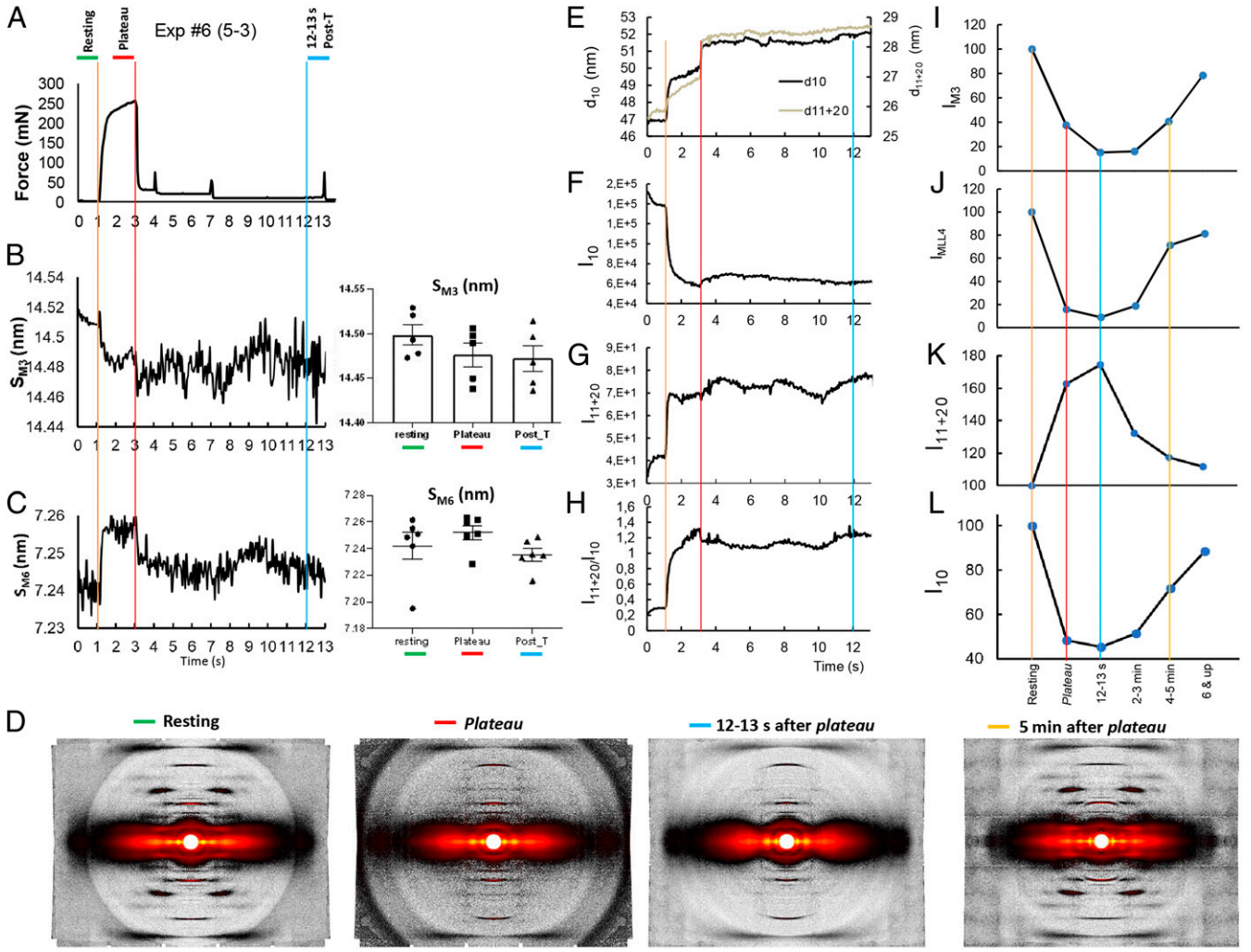

Fig. 5. Time-resolved XRD patterns of an ex vivo femur during a twitch, and before, during, and after a tetanus. (*A*) Force during a supramaximal stimulus train eliciting a pretetanic twitch (not visible due to small size), a 60-Hz 2-s tetanus, and three posttetanic twitches at 4, 7, and 13 s (visible due to potentiation). Time course showing S_{M3} (*B*) and S_{M6} (*C*) changes, with right *Insets* showing statistics (M3 $n = 5$, M6 $n = 6$) in the resting (black circles, green horizontal bar on *A*), plateau (black squares, red bar), and posttetanic (post-T; black triangles, blue bar) 12 to 13 s. (*D*) XRD patterns of resting, plateau, 12 to 13 s and 5 min after plateau (exposure 200 ms each). (*E–H*) Time courses of d_{10} and d_{11} (*E*), I_{10} (*F*), I_{11+20} (*G*), and I_{11+20}/I_{10} ratio (*H*) during 13.5 s. (*I–L*) I_{M3} (*I*), I_{MLL4} (*J*), I_{11+20} (*K*), and I_{10} (*L*) during the resting, tetanic plateau, 12 to 13 s, and 2 to 3, 4 to 5, and 6 min after the end of the tetanus

(58). Here we found that in tarantula muscle after a tetanus I_{MLL4} and I_{10} stayed low, and I_{11} high until 12 to 13 s, slowly returning in >6 min to their initial resting values (Fig. 5 *J–L*). This slow recovery of the original helical arrangement of the myosin heads (several minutes) correlates with the slow dephosphorylation by the endogenous MLCP of first, the Ser45 mono-P swaying BHs, which allows them to dock back helically again to the filament, together with non-P BHs already docked (*SI Appendix*, Fig. S3*B*), and second, the fully released bi-P FHs, so they can dock back as swaying heads on the previously docked BHs, both increasing their contribution to the I_{MLL4} and I_{10} (Fig. 5 *J* and *L*). As with the helical layer lines, the I_{11+20} remains high after the tetanus (Fig. 5*K*), consistent with the bi-P FHs (and some Ser45 mono-P BHs) remaining in the vicinity of the thin filament, recovering slowly to their resting value as dephosphorylation progresses as mentioned before.

Heads that Remain Released and Disordered after a Tetanus Produce PTP. When muscle is stimulated soon after a tetanus, the twitch elicited is substantially stronger than a pretetanic twitch (PTP). It has been proposed that such PTP results from RLC phosphorylation and its accompanying structural effects, in which the myosin heads project from the filament backbone, facilitating their interaction with actin. This structural model has received experimental support from EM studies of isolated thick filaments (27, 30) and XRD of skinned vertebrate and invertebrate muscles (28, 31), but has not been demonstrated in live muscle. Here we have used ex vivo tarantula muscle to correct this deficit.

Fig. 6 shows that early after a tetanus, myosin heads remain disordered (weak I_{MLL4}) and away from the filament backbone (weak I_{10}, strong I_{11+20}, and high I_{11+20}/I_{10}), when almost all heads are still phosphorylated (mono- or bi-) (*SI Appendix*, Fig. S2 *A*, *b* and *B*, *a*). When the muscle is stimulated during this period, the twitch elicited is much stronger than the pretetanus twitch (i.e., exhibits PTP) (Fig. 6 *C* and *D*, force traces, green arrows) and is accompanied in each case by a further increase in I_{11+20} (Fig. 6*A*, red arrows) and I_{11+20}/I_{10} ratio (Fig. 6*C*, red arrows), while disorder remains high (Fig. 6*D*). This can be interpreted straightforwardly in terms of the CPA mechanism, which predicts that following a tetanus, most BHs will be still mono-P and some FHs bi-P, with few non-P heads (Fig. 2 *B*, *e*,

compare with *SI Appendix*, Fig. S2 *A*, *b* and *B*, *a*). The bi-P FHs are disordered and project from the filament backbone, remaining this way until being dephosphorylated to Ser45 mono-P. The mono-P BHs are swaying, spending part of their time, defined by their $[t_{IHM}/(t_{IHM} + t_{rel})]$ duty cycle (see previous section and *SI Appendix*, Fig. S3*D*), on the helical tracks and thus contributing to the layer lines, similar to the swaying FHs in the relaxed pattern. When muscle is stimulated to contract during this time, these heads, already projecting away from the thick filament (reflected in the high I_{11+20} and I_{11+20}/I_{10}) (Fig. 6 *A* and *C*), attach to actin (producing enhanced force, or PTP), shown by a further increase in I_{11+20} and I_{11+20}/I_{10} (Fig. 6 *A* and *C* red arrows). Thus, our experiments suggest that in live muscle a tetanus leads to phosphorylation of many heads (including FH and BH), which continue to project toward the thin filament (phosphorylation "memory") and are therefore readily available for interaction with actin, producing a strong posttetanic twitch. During recovery from the tetanus, RLC phosphorylation gradually returns to baseline through MLCP activity, and we observe a decline in PTP. This follows a return of heads to the thick-filament backbone (I_{11+20} and I_{11+20}/I_{10} drop and I_{10} increases) and restoration of their helical arrangement (I_{MLL4} regains its strength) (Fig. 5 *D* and *J*). We have observed twitch and tetanic tension in freshly dissected muscle where the helical ordering is weak or absent. Thus, helical ordering of the heads establishing the IHM is not a requirement for contraction. Rather, our results show that the highest tension twitches come from heads that are disordered (i.e., during PTP).

Proposed IHM-Based PTP Structural Mechanism for Tarantula. Based on our results and on the dual phosphorylation IHM-based CPA mechanism (Fig. 2*B*), we propose the structural model shown in Fig. 7 to explain force enhancement and PTP in the muscles of tarantula. This mechanism supports the general concepts for phosphorylation-based potentiation advanced previously for fast-twitch vertebrate muscle (22, 23, 43, 60–62), in which it was hypothesized that in live muscle, RLC phosphorylation releases the heads, similarly to what was found in isolated thick filaments and skinned muscle in tarantula (27, 28), *Limulus* (29), and rabbit (30, 31), thus facilitating their attachment to actin, providing an explanation for potentiation both during and after a tetanus (as PTP). The model, which includes the constraints of the tarantula thick-filament structure (34), suggests a specific structural mechanism that explains: 1) Force enhancement during a tetanus by recruiting additional bi-P FHs and Ser45 mono-P BHs (Fig. 7*C* vs. Fig. 7*B*), grading (i.e., potentiating) the achieved force, and 2) the PTP phenomenon (compare Fig. 7*E* vs. Fig. 7*B*), consistent with our experimental XRD (Figs. 5 and 6) and U-G results (*SI Appendix*, Fig. S2 *A*, *b* and *B*, *a*).

Arthropod striated muscles share similar thick-filament head arrangements and long RLC NTEs with dual PKC/MLCK phosphorylation sites. Apart from tarantula, RLC phosphorylation has been reported in *Limulus* (24), and PTP in scorpion (63), whose thick filaments (25, 64) are similar to tarantula. Therefore, the proposed mechanism could, in principle, be extended to the other species exhibiting long RLC NTEs with PKC/MLCK consensus sequences. RLC phosphorylation remaining after a tetanus has been reported in frog (65), rabbit (66), and mouse (62). Residual I_{MLL1} after a tetanus has been observed in frog (55, 56) and mouse (57). Here we have associated, in intact tarantula muscle, residual RLC phosphorylation (*SI Appendix*, Fig. S2 *A*, *a* and *B*, *a*), residual I_{MLL1} and I_{MLL4}, and residual released and disordered heads after a tetanus, with PTP (Fig. 7). Can the mechanism shown in Fig. 7 be extended as well to explain PTP in vertebrate muscles? Brito et al. (34) reported that vertebrate muscle RLCs exhibit only short NTEs, with MLCK consensus sequences and only one MLCK-phosphorylatable serine. Therefore, the proposed mechanism could be extended to vertebrate muscle but modified for allowing only mono-phosphorylation. Mono-PKC–phosphorylated, swaying heads in tarantula would correspond to the constitutively ON (non-phosphorylated) heads in vertebrate (1). In tarantula the recovery

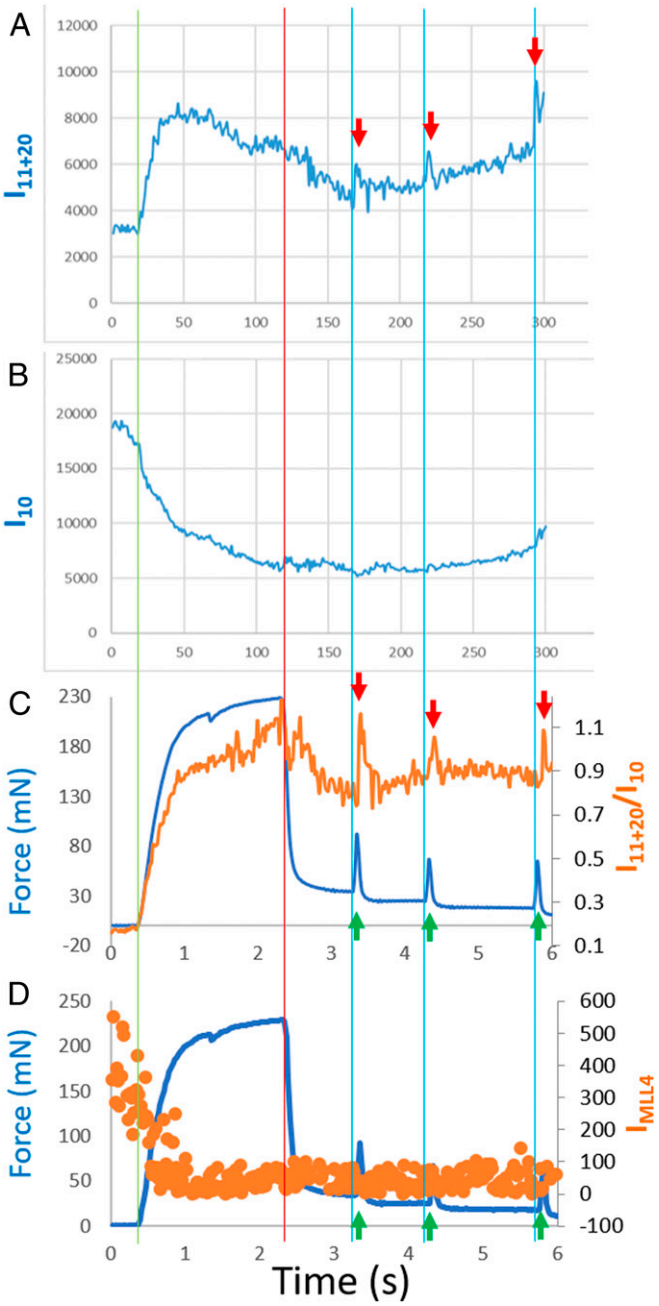

Fig. 6. Time-resolved XRD patterns of a PTP experiment. Time courses of the I_{11+20} (*A*), I_{10} (*B*), I_{11+20}/I_{10} ratio (*C*), and I_{MLL4} (*D*) during a pretetanic twitch (not visible due to small size), 2-s 60-Hz tetanus (recorded force shown in blue in *C* and *D*), and three PTP twitches (shown in blue in *C* and *D*, green arrows), showing that early after a tetanus, myosin heads remain disordered (weak I_{MLL4}) and away from the filament backbone (weak I_{10}, strong I_{11+20}, and high I_{11+20}/I_{10}); during this time, almost all heads are phosphorylated (mono- or bi-). The pretetanic twitch (0.4 mN) was barely above the force transducer (resolution of ~1 mN) baseline. The first posttetanic twitch (57 mN) was potentiated ~50 times. When the muscle is stimulated during this period, the twitch elicited is much stronger than the pretetanus twitch (i.e., exhibits PTP) and is accompanied in each case by a further increase in I_{11+20} (red arrows) and I_{11+20}/I_{10} (red arrows), whereas disorder (weak I_{MLL4}) remains high.

phase after a tetanus implies a slow dephosphorylation time τ (minutes) of the mono-P and bi-P heads (Fig. 7, *Inset*), that by remaining released and disordered "memorize" the previous muscle history. In vertebrates, this could be accomplished more quickly as the PTP recovery would involve the dephosphorylation time of only mono-P heads. Brito et al. (34) also reported that some species that show direct Ca^{2+}-activation via the RLC, like scallop (67), exhibit RLCs with only short NTEs and a single serine, with no MLCK consensus sequence, suggesting that a phosphorylation-based mechanism like the IHM-based CPA mechanism (Fig. 2) and the PTP mechanism (Fig. 7) cannot be functional for them.

Evolution Has Resulted in Different Thick-Filament Activation Mechanisms. Different molecular mechanisms for activation have evolved to control the release and disordering of myosin heads in striated muscles in order to actively recruit them to produce force: 1) Direct Ca^{2+}-binding, 2) RLC phosphorylation, 3) mechanosensing, and 4) delayed stretch activation. Mechanosensing (Fig. 8*C*) is a prominent feature of vertebrate skeletal muscle (1). Here we show evidence (Figs. 5 and 6 and *SI Appendix*, Fig. S2) that in tarantula there is a primary phosphorylation mechanism (Fig. 8*B*), with at most a subsidiary role for mechanosensing because the lengthening of the backbone was much smaller (and statistically not significant) than in frog. In tarantula muscle, during a twitch, the swaying heads (due to their mono-P at Ser35) are intermittently extended ready to bind to Ca^{2+}-activated thin filaments to produce initial force, and phosphorylation releases more heads. In frog, lacking constitutive phosphorylation, constitutively ON heads develop initial force, and inactive heads are then released by mechanosensing as force increases. In both muscles, PTP is due to RLC phosphorylation, possibly differing in how long the PTP lasts. Another important difference between the thick filaments of invertebrates and vertebrates is the presence of PM in the invertebrate filament backbone, suggesting that the lack of backbone lengthening in tarantula may be associated with the rigidity of its thick filaments, due to a core of tightly packed PM molecules (Fig. 1 *B*, *d*), in contrast to frog that lacks this rigid core. Some of these mechanisms may be widespread, such as the dual phosphorylation CPA mechanism in Arthropoda, with single phosphorylation variations present in vertebrate muscle as a modulatory mechanism. Other activation mechanisms are very specific, such as the Ca^{2+}-binding activation mechanism, observed only in mollusks (Fig. 8*A*), and the stretch activation observed in the indirect flight muscles of *Lethocerus* and other flying insects. So far, mechanosensing appears to be confined to vertebrates.

We conclude that the molecular mechanisms of thick filament activation and PTP evolved differently in invertebrate and vertebrate striated muscle as adaptations to the lifestyle of the

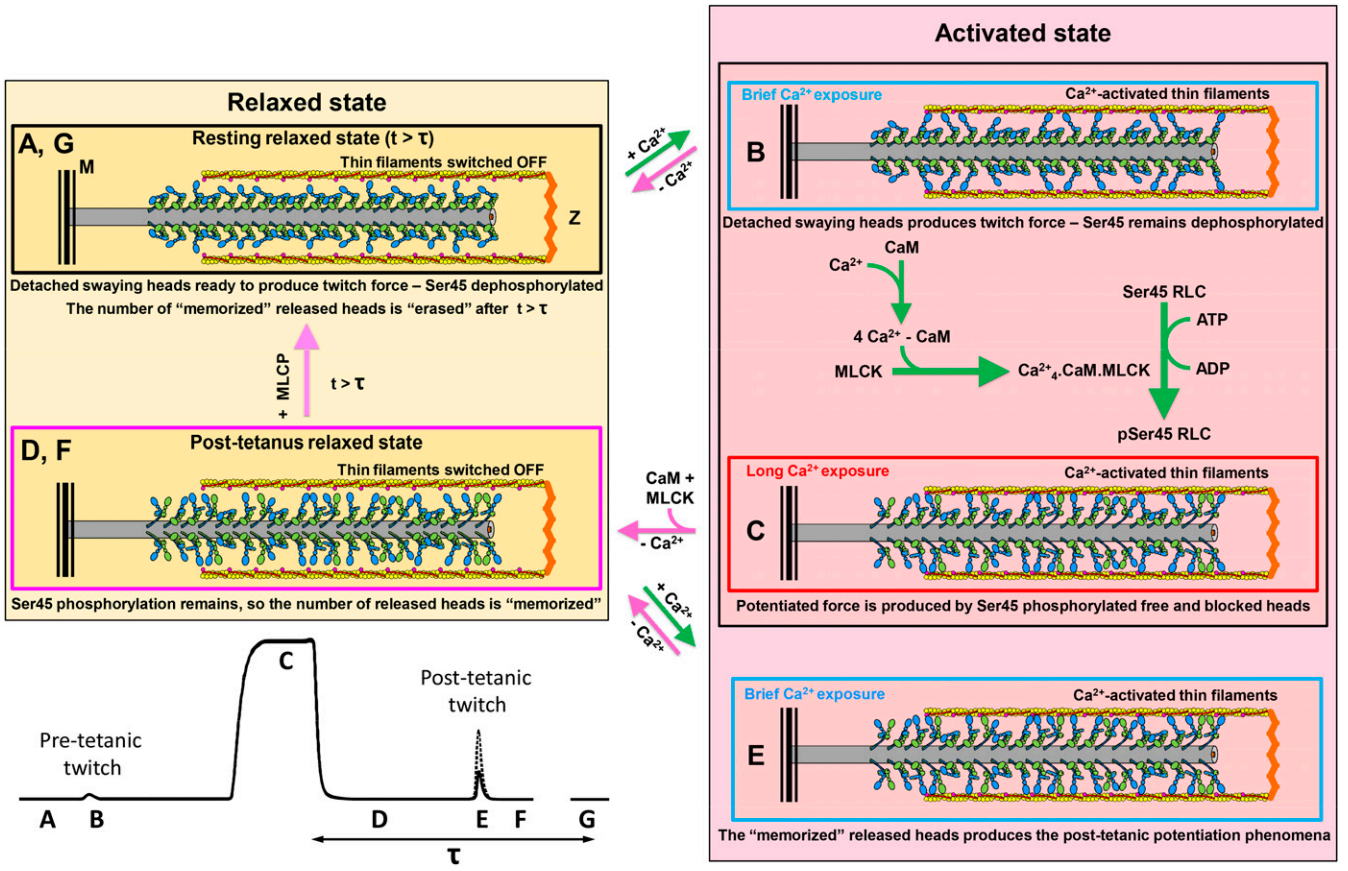

Fig. 7. Model explaining PTP in tarantula, based on the IHM-based CPA mechanism. In relaxation (*A*) [Ca^{2+}] is low so thin filaments and MLCK are switched OFF while MLCP, always on, dephosphorylates any phosphorylated Ser45. On activation, [Ca^{2+}] is high, switching on thin filaments and MLCK. With brief high [Ca^{2+}] exposure (twitches) (*B*), Ser35 mono-P swaying FHs bind to thin filaments producing force, while few FHs can be bi-P. On longer high [Ca^{2+}] exposure (tetani) (*C*), MLCK can bi-P FHs and Ser45 mono-P some BHs. After tetanus, [Ca^{2+}] is low, switching off thin filaments and MLCK. In posttetanus relaxation (*D*) bi-P FHs remain released and Ser45 mono-P BHs sway away until dephosphorylated by MLCP (time τ), and resting relaxation is recovered (*G*). If, in this state (*D*), a brief high [Ca^{2+}] exposure occurs, bi-P FHs and Ser45 mono-P BHs (not yet dephosphorylated by MLCP) remain released or swaying away, bind to switched ON thin filaments, producing greater force (*E*) than pretetanic (*B*), structurally explaining PTP "memory."

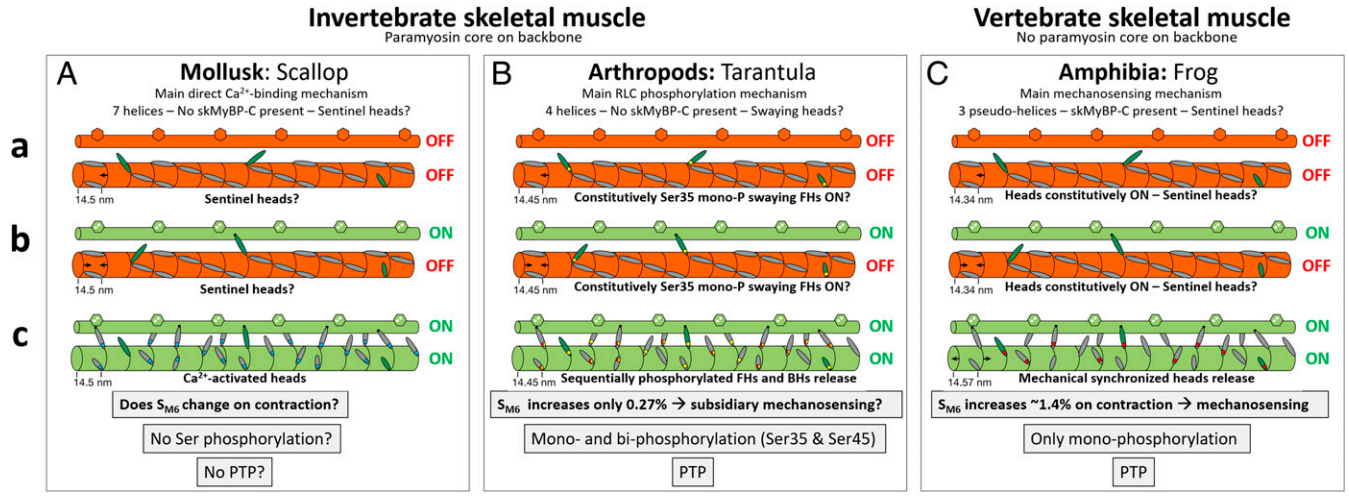

Fig. 8. Dual-filament regulation in invertebrate and vertebrate muscles could be associated with the presence of PM in the thick-filament backbone core. Thick filaments containing PM (scallop, tarantula) or not (frog) are activated either (*A*) directly by Ca^{2+} (blue circles), (*B*) by PKC/MLCK Ser35/Ser45 dual phosphorylation (circles in yellow: Ser35 mono-P, red: Ser45 mono-P, yellow/red: bi-P), or (*C*) mechanosensing. Thick and thin filaments are shown either switched OFF (orange) or ON (green), in relaxed (*a*) or contracting without load (*b*) or with load (*c*). Based on Linari et al. (1).

organisms. Our results support the notion that helically ordered IHMs are the key to energy conservation in the resting relaxed state, brought about by the interactions between the heads that inhibit their activity (20). In tarantula live muscle, while the ATP turnover rates for the swaying FHs is either slow (250 to 300 s) while being transiently attached forming helices or fast (<30 s) while being transiently detached and disordered (20, 54), an important fraction of the heads (BHs)—permanently docked forming helices on the filament—exhibit a very slow ATP turnover rate (1,800 s), an energy conserving state. Force potentiation both during and after a tetanus in tarantula muscle could be a way to increase force when needed, according to the previous muscle activation history (PTP), while saving ATP when not (54), which could be energetically favorable in an arthropod that spends large amounts of time immobile, with only occasional bursts of energy required for moving when capturing food or avoiding predators, among other vital activities.

A key point to note is the existence of two different relaxed states that are structurally distinct: 1) The "resting" relaxed state in which heads are helically ordered in the IHM, with minimal usage of ATP (possibly equivalent to the superrelaxed state); and 2) the "posttetanic" relaxed state, in which heads are in a disordered, preactivated, non-IHM state, near to actin. Both states are mechanically relaxed, and the thin filaments are switched off. These states, determined experimentally, may correlate with different phases of the daily life of the tarantula. The animal spends most of its time at rest, hidden and motionless, conserving energy (resting relaxed state). When the need to capture food or escape a predator arises, the muscles become active and RLC phosphorylation is initiated, leading to enhanced force production. Relaxation still occurs when the thin filaments are switched off between contractions (posttetanic relaxed state), but more force is produced upon activation, as many heads are already near actin. Energy conservation is lower during these relaxed intervals but that is less important than having high force when needed. When activity ceases, the muscles return to their resting relaxed state.

Tarantula provides an excellent model system for understanding thick-filament structure and function in terms of the BHs and FHs of the IHM. EM yields key insights into the organization of the two heads in the IHM in the static state of relaxation, including their interactions, relative stability, and accessibility of their RLC phosphorylatable serines (8, 34, 35). XRD complements these studies, demonstrating the presence of this same IHM arrangement in intact muscle, and additionally revealing dynamic changes in the heads that underlie activation and potentiation. These studies suggest very different roles and dynamics for BHs and FHs in tarantula. A similar distinction between heads might also occur in vertebrate muscle, where the IHM is also present (68). Previous studies indicate a residual population of helically ordered heads in activated muscles, but not assigned to any particular head (blocked or free) (55–57). Our tarantula observations would suggest that the majority of residual ordered heads would be BHs, and that any constitutively active heads would come from the FH population.

Materials and Methods

X-Ray Diffraction. Legs were excised from anesthetized Texas brown tarantulas and placed in an X-ray chamber. Muscles were stimulated through platinum electrodes using an Aurora Scientific 701A stimulator. XRD patterns from muscles in resting or activated states were obtained at the Advanced Photon Source, Argonne National Laboratory, and recorded on a Pilatus 3 1M detector (Dectris Inc.) with 20-ms exposures and 50 ms between exposures. For in vivo experiments, the live tarantula was constrained in a plastic tube mounted in the X-ray beam.

XRD Pattern Modeling. Fourier transforms were calculated for the thick filaments assuming a myosin head spacing of 14.5 nm, a helical repeat of 43.5 nm, and fourfold rotational symmetry.

U-G gel electrophoresis was carried out according to Sulbarán et al. (35) on muscles frozen at the end of the tetanic plateau.

Full details of methods are provided in *SI Appendix*.

Data Availability. Data were deposited in the Open Science Framework, https://osf.io/anxuy/?view_only=5491c6ba8bca4add9d97930614734e0e.

ACKNOWLEDGMENTS. We thank Dr. Carlo Caputo for advice and Dr. Michael Previs for suggestions. Research was supported by National Institutes of Health Grants National Institute of General Medical Sciences GM103622 (to T.I.), National Heart, Lung, and Blood Institute HL139883 (to Richard Moss and R.C.), National Institute of Arthritis and Musculoskeletal and Skin Diseases AR072036 (to R.C.), AR067279 (to R.C. and D. Warshaw), Office of Research Infrastructure Programs 1S10OD018090-01 (to T.I.), and Russia State Program AAAA-A19-119012990119-3 (to N.K. and A.T.). The Advanced Photon Source is operated for the Department of Energy Office of Science by Argonne National Laboratory under Contract DE-AC02-06CH11357. The content of this work is solely the responsibility of the authors and does not necessarily reflect the official views of the National Institutes of Health.

1. M. Linari *et al*., Force generation by skeletal muscle is controlled by mechanosensing in myosin filaments. *Nature* **528**, 276–279 (2015).
2. H. E. Huxley, Electron microscope studies on the structure of natural and synthetic protein filaments from striated muscle. *J. Mol. Biol.* **7**, 281–308 (1963).
3. R. W. Kensler, R. J. Levine, An electron microscopic and optical diffraction analysis of the structure of Limulus telson muscle thick filaments. *J. Cell Biol.* **92**, 443–451 (1982).
4. H. E. Huxley, W. Brown, The low-angle X-ray diagram of vertebrate striated muscle and its behaviour during contraction and rigor. *J. Mol. Biol.* **30**, 383–434 (1967).
5. J. S. Wray, P. J. Vibert, C. Cohen, Diversity of cross-bridge configurations in invertebrate muscles. *Nature* **257**, 561–564 (1975).
6. J. S. Wray, Organization of myosin in invertebrate thick filaments. *Soc. Gen. Physiol. Ser.* **37**, 29–36 (1982).
7. R. W. Kensler, M. Stewart, Frog skeletal muscle thick filaments are three-stranded. *J. Cell Biol.* **96**, 1797–1802 (1983).
8. J. L. Woodhead *et al*., Atomic model of a myosin filament in the relaxed state. *Nature* **436**, 1195–1199 (2005).
9. L. Alamo *et al*., Three-dimensional reconstruction of tarantula myosin filaments suggests how phosphorylation may regulate myosin activity. *J. Mol. Biol.* **384**, 780–797 (2008).
10. T. Wendt, D. Taylor, K. M. Trybus, K. Taylor, Three-dimensional image reconstruction of dephosphorylated smooth muscle heavy meromyosin reveals asymmetry in the interaction between myosin heads and placement of subfragment 2. *Proc. Natl. Acad. Sci. U.S.A.* **98**, 4361–4366 (2001).
11. S. A. Burgess *et al*., Structures of smooth muscle myosin and heavy meromyosin in the folded, shutdown state. *J. Mol. Biol.* **372**, 1165–1178 (2007).
12. S. Xu, G. Offer, J. Gu, H. D. White, L. C. Yu, Temperature and ligand dependence of conformation and helical order in myosin filaments. *Biochemistry* **42**, 390–401 (2003).
13. M. E. Zoghbi, J. L. Woodhead, R. Craig, R. Padrón, Helical order in tarantula thick filaments requires the "closed" conformation of the myosin head. *J. Mol. Biol.* **342**, 1223–1236 (2004).
14. H. S. Jung, S. Komatsu, M. Ikebe, R. Craig, Head-head and head-tail interaction: A general mechanism for switching off myosin II activity in cells. *Mol. Biol. Cell* **19**, 3234–3242 (2008).
15. K. H. Lee *et al*., Interacting-heads motif has been conserved as a mechanism of myosin II inhibition since before the origin of animals. *Proc. Natl. Acad. Sci. U.S.A.* **115**, E1991–E2000 (2018).
16. L. Alamo, A. Pinto, G. Sulbarán, J. Mavárez, R. Padrón, Lessons from a tarantula: New insights into myosin interacting-heads motif evolution and its implications on disease. *Biophys. Rev.* **10**, 1465–1477 (2018).
17. Z. Hu, D. W. Taylor, M. K. Reedy, R. J. Edwards, K. A. Taylor, Structure of myosin filaments from relaxed *Lethocerus* flight muscle by cryo-EM at 6 Å resolution. *Sci. Adv.* **2**, e1600058 (2016).
18. M. A. Stewart, K. Franks-Skiba, S. Chen, R. Cooke, Myosin ATP turnover rate is a mechanism involved in thermogenesis in resting skeletal muscle fibers. *Proc. Natl. Acad. Sci. U.S.A.* **107**, 430–435 (2010).
19. L. Alamo *et al*., Effects of myosin variants on interacting-heads motif explain distinct hypertrophic and dilated cardiomyopathy phenotypes. *eLife* **6**, e24634 (2017).
20. L. Alamo *et al*., Conserved intramolecular interactions maintain myosin interacting-heads motifs explaining tarantula muscle super-relaxed state structural basis. *J. Mol. Biol.* **428**, 1142–1164 (2016).
21. L. Alamo *et al*., Lessons from a tarantula: New insights into muscle thick filament and myosin interacting-heads motif structure and function. *Biophys. Rev.* **9**, 461–480 (2017).
22. H. L. Sweeney, B. F. Bowman, J. T. Stull, Myosin light chain phosphorylation in vertebrate striated muscle: Regulation and function. *Am. J. Physiol.* **264**, C1085–C1095 (1993).
23. R. Vandenboom, Modulation of skeletal muscle contraction by myosin phosphorylation. *Compr. Physiol.* **7**, 171–212 (2016).
24. J. R. Sellers, Phosphorylation-dependent regulation of Limulus myosin. *J. Biol. Chem.* **256**, 9274–9278 (1981).
25. F. Q. Zhao, R. Craig, J. L. Woodhead, Head-head interaction characterizes the relaxed state of Limulus muscle myosin filaments. *J. Mol. Biol.* **385**, 423–431 (2009).
26. J. T. Stull, D. R. Manning, C. W. High, D. K. Blumenthal, Phosphorylation of contractile proteins in heart and skeletal muscle. *Fed. Proc.* **39**, 1552–1557 (1980).
27. R. Craig, R. Padrón, J. Kendrick-Jones, Structural changes accompanying phosphorylation of tarantula muscle myosin filaments. *J. Cell Biol.* **105**, 1319–1327 (1987).
28. R. Padrón, N. Panté, H. Sosa, J. Kendrick-Jones, X-ray diffraction study of the structural changes accompanying phosphorylation of tarantula muscle. *J. Muscle Res. Cell Motil.* **12**, 235–241 (1991).
29. R. J. Levine, P. D. Chantler, R. W. Kensler, J. L. Woodhead, Effects of phosphorylation by myosin light chain kinase on the structure of Limulus thick filaments. *J. Cell Biol.* **113**, 563–572 (1991).
30. R. J. Levine, R. W. Kensler, Z. Yang, J. T. Stull, H. L. Sweeney, Myosin light chain phosphorylation affects the structure of rabbit skeletal muscle thick filaments. *Biophys. J.* **71**, 898–907 (1996).
31. M. Yamaguchi *et al*., X-ray diffraction analysis of the effects of myosin regulatory light chain phosphorylation and butanedione monoxime on skinned skeletal muscle fibers. *Am. J. Physiol. Cell Physiol.* **310**, C692–C700 (2016).
32. R. Craig, W. Lehman, Crossbridge and tropomyosin positions observed in native, interacting thick and thin filaments. *J. Mol. Biol.* **311**, 1027–1036 (2001).
33. C. Hidalgo, R. Craig, M. Ikebe, R. Padrón, Mechanism of phosphorylation of the regulatory light chain of myosin from tarantula striated muscle. *J. Muscle Res. Cell Motil.* **22**, 51–59 (2001).
34. R. Brito *et al*., A molecular model of phosphorylation-based activation and potentiation of tarantula muscle thick filaments. *J. Mol. Biol.* **414**, 44–61 (2011).
35. G. Sulbarán *et al*., Different head environments in tarantula thick filaments support a cooperative activation process. *Biophys. J.* **105**, 2114–2122 (2013).
36. G. Sulbarán *et al*., (18)O labeling on Ser45 but not on Ser35 supports the cooperative phosphorylation mechanism on tarantula thick filament activation. *Biochem. Biophys. Res. Commun.* **524**, 198–204 (2020).
37. J. L. Woodhead, R. Craig, Through thick and thin—Interfilament communication in muscle. *Biophys. J.* **109**, 665–667 (2015).
38. M. J. Previs, S. Beck Previs, J. Gulick, J. Robbins, D. M. Warshaw, Molecular mechanics of cardiac myosin-binding protein C in native thick filaments. *Science* **337**, 1215–1218 (2012).
39. L. M. Espinoza-Fonseca, L. Alamo, A. Pinto, D. D. Thomas, R. Padrón, Sequential myosin phosphorylation activates tarantula thick filament via a disorder-order transition. *Mol. Biosyst.* **11**, 2167–2179 (2015).
40. L. Alamo *et al*., Tarantula myosin free head regulatory light chain phosphorylation stiffens N-terminal extension, releasing it and blocking its docking back. *Mol. Biosyst.* **11**, 2180–2189 (2015).
41. J. Ranke, *Tetanus: Eine Physiologische Studie* (Wilhelm Engelmann, Leipzig, Germany, ed. 1, 1865).
42. R. Close, J. F. Hoh, The after-effects of repetitive stimulation on the isometric twitch contraction of rat fast skeletal muscle. *J. Physiol.* **197**, 461–477 (1968).
43. J. T. Stull, K. E. Kamm, R. Vandenboom, Myosin light chain kinase and the role of myosin light chain phosphorylation in skeletal muscle. *Arch. Biochem. Biophys.* **510**, 120–128 (2011).
44. A. J. Blazevich, N. Babault, Post-activation potentiation versus post-activation perfomance enhancement in humans: Historical perspective, underlying mechanisms, and current issues. *Front. Physiol.* **10**, 1359 (2019).
45. N. A. Koubassova, A. K. Tsaturyan, Direct modeling of X-ray diffraction pattern from skeletal muscle in rigor. *Biophys. J.* **83**, 1082–1097 (2002).
46. R. T. Tregear, J. Hoyland, A. J. Sayers, The repeat distance of myosin in the thick filaments of various muscles. *J. Mol. Biol.* **176**, 417–420 (1984).
47. R. A. Crowther, R. Padrón, R. Craig, Arrangement of the heads of myosin in relaxed thick filaments from tarantula muscle. *J. Mol. Biol.* **184**, 429–439 (1985).
48. E. Rome, Structural studies by X-ray diffraction of striated muscle permeated with certain ions and proteins. *Cold Spring Harb. Symp. Quant. Biol.* **37**, 331–339 (1973).
49. M. Linari *et al*., Interference fine structure and sarcomere length dependence of the axial X-ray pattern from active single muscle fibers. *Proc. Natl. Acad. Sci. U.S.A.* **97**, 7226–7231 (2000).
50. J. Zhu *et al*., Analysis of tarantula skeletal muscle protein sequences and identification of transcriptional isoforms. *BMC Genom.* **10**, 117 (2009).
51. S. Yang, J. L. Woodhead, F. Q. Zhao, G. Sulbaran, R. Craig, An approach to improve the resolution of helical filaments with a large axial rise and flexible subunits. *J. Struct. Biol.* **193**, 45–54 (2016).
52. C. Knupp, E. Morris, J. M. Squire, The interacting head motif structure does not explain the X-ray diffraction patterns in relaxed vertebrate (bony fish) skeletal muscle and insect (*Lethocerus*) flight muscle. *Biology* **8**, 67 (2019).
53. P. R. Steinmetz *et al*., Independent evolution of striated muscles in cnidarians and bilaterians. *Nature* **487**, 231–234 (2012).
54. N. Naber, R. Cooke, E. Pate, Slow myosin ATP turnover in the super-relaxed state in tarantula muscle. *J. Mol. Biol.* **411**, 943–950 (2011).
55. H. E. Huxley, A. R. Faruqi, M. Kress, J. Bordas, M. H. Koch, Time-resolved X-ray diffraction studies of the myosin layer-line reflections during muscle contraction. *J. Mol. Biol.* **158**, 637–684 (1982).
56. H. Tanaka, T. Kobayashi, Y. Amemiya, K. Wakabayashi, Time-resolved X-ray diffraction studies of frog skeletal muscle isometrically twitched by two successive stimuli using synchrotron radiation. *Biophys. Chem.* **25**, 161–168 (1986).
57. W. Ma, H. Gong, T. Irving, Myosin head configurations in resting and contracting murine skeletal muscle. *Int. J. Mol. Sci.* **19**, 2643 (2018).
58. H. E. Huxley, Structural changes in the actin- and myosin-containing filaments during contraction. *Cold Spring Harb. Symp. Quant. Biol.* **37**, 361–376 (1973).
59. N. Yagi, M. H. Ito, H. Nakajima, T. Izumi, I. Matsubara, Return of myosin heads to thick filaments after muscle contraction. *Science* **197**, 685–687 (1977).
60. D. R. Manning, J. T. Stull, Myosin light chain phosphorylation and phosphorylase A activity in rat extensor digitorum longus muscle. *Biochem. Biophys. Res. Commun.* **90**, 164–170 (1979).
61. G. Zhi *et al*., Myosin light chain kinase and myosin phosphorylation effect frequency-dependent potentiation of skeletal muscle contraction. *Proc. Natl. Acad. Sci. U.S.A.* **102**, 17519–17524 (2005).
62. R. Vandenboom, W. Gittings, I. C. Smith, R. W. Grange, J. T. Stull, Myosin phosphorylation and force potentiation in skeletal muscle: Evidence from animal models. *J. Muscle Res. Cell Motil.* **34**, 317–332 (2013).
63. W. F. Gilly, T. Scheuer, Contractile activation in scorpion striated muscle fibers. Dependence on voltage and external calcium. *J. Gen. Physiol.* **84**, 321–345 (1984).
64. A. Pinto, F. Sánchez, L. Alamo, R. Padrón, The myosin interacting-heads motif is present in the relaxed thick filament of the striated muscle of scorpion. *J. Struct. Biol.* **180**, 469–478 (2012).
65. K. Bárány, M. Bárány, Phosphorylation of the 18,000-dalton light chain of myosin during a single tetanus of frog muscle. *J. Biol. Chem.* **252**, 4752–4754 (1977).
66. C. J. Ritz-Gold, R. Cooke, D. K. Blumenthal, J. T. Stull, Light chain phosphorylation alters the conformation of skeletal muscle myosin. *Biochem. Biophys. Res. Commun.* **93**, 209–214 (1980).
67. A. G. Szent-Györgyi, Regulation by myosin: How calcium regulates some myosins, past and present. *Adv. Exp. Med. Biol.* **592**, 253–264 (2007).
68. M. E. Zoghbi, J. L. Woodhead, R. L. Moss, R. Craig, Three-dimensional structure of vertebrate cardiac muscle myosin filaments. *Proc. Natl. Acad. Sci. U.S.A.* **105**, 2386–2390 (2008).